International Journal of Engineering Research & Technology (IJERT)
ISSN: 2278-0181
Vol. 15 Issue 08 , August - 2026

# Microwave-Assisted Synthesis and Characterization of Ag-Doped $TiO_2$ for Photocatalytic Treatment of Carwash Wastewater

Shivalini Singh, Ashish Kumar, Himani Pachauri, Mohammad Mudassir
Department of Chemistry, Agra College, Agra
(Dr. Bhim Rao Ambedkar University, Agra – 282001)

**Abstract - Carwash wastewater, carries a heavy dissolved organic load (COD 620 mg/L, TOC 51.4 mg/L, $UV_{254}$ 2.066 $cm^{-1}$, pH 7.6, turbidity 20 NTU) resistant to conventional treatment. Undoped $TiO_2$ and 0.5 wt.% Ag-doped $TiO_2$ photocatalyst, synthesised via a microwave-assisted, agar-agar-templated sol–gel route (calcined 700 °C, 3 h), were tested as photocatalysts for its degradation under UV-C irradiation across three catalyst doses (10–50 mg/100 mL) and four irradiation times (0–180 min), with TOC, COD and $UV_{254}$ tracked in triplicate. Control experiments confirmed that photocatalysis, not adsorption (≤14.1%) or direct photolysis (≤19.6%), drove removal. At the optimal dose (50 mg/100 mL, 180 min), 0.5% Ag–$TiO_2$ far outperformed undoped $TiO_2$ (TOC 77.0% vs. 37.7%; COD 88.0% vs. 48.6%; $UV_{254}$ 91.2% vs. 53.3%). Pseudo-first-order kinetics gave a $UV_{254}$ rate constant for 0.5% Ag–$TiO_2$ over three times higher than undoped $TiO_2$ (13.10 vs. 4.25 × $10^{-3}$ $min^{-1}$).The superior performance of 0.5% Ag–$TiO_2$ is attributed to a substantially higher anatase retention (64.8 wt% anatase / 35.2 wt% rutile, versus 29.6/70.4 for undoped $TiO_2$, by Spurr–Myers analysis of the raw XRD data), a marginally smaller crystallite size (Williamson–Hall anatase 34.0 nm vs. 34.1 nm and rutile 46.7 nm vs. 48.3 nm), and a narrowed, markedly flattened optical band gap (2.82 eV vs. 2.96 eV by Tauc analysis of UV–Vis diffuse reflectance spectra), which together are consistent with improved charge separation, a higher density of photocatalytically favourable anatase sites, and a persistent, non-plasmonic visible-light absorption background. HRTEM lattice-fringe analysis corroborated the anatase-dominant character of Ag-doped $TiO_2$ catalysts at the particle level. These findings identify 0.5% Ag–$TiO_2$ as an effective, low-cost photocatalyst for the advanced oxidation treatment of carwash wastewater.**

***Keywords*** **- $TiO_2$ photocatalysis; silver doping; carwash wastewater treatment; sol–gel synthesis; Agar-Agar; XRD**

## 1. INTRODUCTION

Water scarcity and degradation of water quality are among the most pressing environmental issues of the twenty-first century and industrial and commercial service sectors are increasingly being scrutinized as contributors to these problems. In particular, the vehicle-washing industry produces large quantities of wastewater, with reported consumption often exceeding 250–300 litres/vehicle, depending on the washing technology employed (Fall et al., 2007). Although this effluent is frequently colourless and visually unremarkable, it contains a considerable dissolved and colloidal organic load, including detergent surfactants, oils, greases, and residues washed from vehicle surfaces. These substances are not mineralizable by conventional primary treatment methods such as sedimentation, screening or coagulation-flocculation (Bhatti et al., 2011; Sarmadi et al., 2020). Advanced oxidation processes are particularly suitable for this purpose because their reactive species can attack organic compounds through successive oxidation reactions with relatively low selectivity. (Ganiyu, 2018).

Photocatalytic oxidation provides an attractive route for treating such complex organic mixtures, with $TiO_2$ being one of the most widely investigated semiconductor photocatalysts. Its chemical inertness, resistance to photo-corrosion, availability, and ability to generate strongly oxidising surface species have made it particularly relevant for degrading organic contaminants. The practical effectiveness of $TiO_2$, however, depends strongly on the fate of the photogenerated charge carriers. Its wide band gap (approximately 3.0–3.2 eV) limits photon utilisation mainly to the UV range, while rapid electron–hole recombination reduces the number of carriers that can participate in surface oxidation reactions (Chakhtouna et al., 2021). Modification of the $TiO_2$ surface or lattice with suitable metals has consequently become an important strategy for improving photocatalytic charge utilisation (Rabhi et al., 2019; Singh & Kumar, 2021).

International Journal of Engineering Research & Technology (IJERT)
ISSN: 2278-0181
Vol. 15 Issue 08 , August - 2026

Silver is of particular interest in this context due to its interaction with $TiO_2$ that can produce desirable interfacial charge-transfer pathways. Ag species deposited or incorporated onto $TiO_2$ can serve as electron-accepting sites, which facilitate charge separation and therefore enhance the probability of the participation of photogenerated holes and electrons in surface reactions rather than their recombination. The alteration of the electronic structure and the surface charge behavior can favor the generation of reactive species involved in the oxidation of organic pollutants (Chakhtouna et al., 2021). In addition to these electronic effects, the presence of silver may also influence the crystallization and thermal evolution of $TiO_2$. The preparation conditions are therefore important to determine the final photocatalytic properties.

Because the structural and surface properties of $TiO_2$ are strongly influenced by the synthesis route, considerable attention has also been directed toward rapid and controlled preparation methods. The microwave-assisted sol–gel method offers advantages over prolonged conventional heating because microwave irradiation can provide rapid and volumetric heating, thereby shorten processing time and potentially improve control over nucleation and particle growth. Microwave-assisted sol–gel approaches have been successfully employed for the preparation of $TiO_2$-based photocatalysts and have been associated with control over crystallite size, morphology, and phase composition (Imoisili et al., 2021; Hernández et al., 2020). In addition to microwave irradiation, the incorporation of a biopolymer-derived structure-directing or capping material can provide another means of controlling the development of $TiO_2$ nanoparticles. Agar-based materials are attractive for this purpose because of their low cost, availability, and ability to interact with precursor species during gel formation and subsequent thermal treatment. Such organic templates can influence nucleation, particle growth, aggregation, and the resulting surface characteristics of oxide nanomaterials (Lu et al., 2021). Thus, combining a sol–gel route with microwave-assisted processing and agar-agar templating provides a potentially effective strategy for obtaining finely structured $TiO_2$-based photocatalysts with properties suitable for the oxidative degradation of organic constituents in carwash wastewater.

In the present study, we describe the doping of $TiO_2$ with Ag via microwave assisted, Agar-Agar-Templated Sol–Gel Route. The synthesized nanomaterials were thoroughly characterized by XRD, HRTEM and UV-vis DRS. The effects of doping and calcination temperature on the photocatalytic activity of photocatalysts were studied. The photocatalytic activity of the catalyst was evaluated by using carwash wastewater organic pollutant. In order to achieve maximum photocatalytic activity, a series of experiments were carried out which includes the content of silver doping, effect of catalyst loading rationalise the observed performance gap in terms of the underlying phase composition and charge-separation mechanism.

## 2. EXPERIMENTAL

### *2.1 Materials*

All the materials used in this work are of analytical reagent grade. Titanium tetra-isopropoxide (TTIP, Ti $[OCH(CH_3)_2]_4$), silver nitrate ($AgNO_3$), isopropyl alcohol, deionized water, concentrated nitric acid and Agar-agar as a biodegradable templating and capping agent.

### *2.2 Synthesis of Catalyst*

Silver doped $TiO_2$ catalyst were prepared by sol-gel method. Under continuous stirring, 0.5% of silver nitrate ($AgNO_3$) were previously dissolved in a mixture solution consisting of 24.1 mL isopropyl alcohol, 3 mL deionized water, and 0.3 mL nitric acid to form the mixture solution A. Then solution A was added dropwise into the mixture solution B containing 10.65 mL titanium tetra-isopropoxide and 24.1 mL isopropyl alcohol. The obtained homogeneous solution was stirred continuously for 1 h to form a gel (Huang et al., 2015). Then agar-agar solution was added to it and again stirred for 15 min. The gel was then subjected to microwave irradiation for 20 min, with on–off cycle (15s on–40s off) (Suwarnkar et al., 2014). The dry gel was calcined in a muffle furnace at 700°C for 3hrs. to obtain 0.5% Ag-doped $TiO_2$. The same process was followed for synthesis of the undoped catalyst.

### *2.3 Catalyst Characterisation*

Both catalysts were characterized by X-ray diffraction (XRD; Cu Kα radiation, $\lambda = 1.54059$ Å, $2\theta = 2\text{-}90°$) by Debye-Scherrer and Williamson-Hall analysis to determine the crystallite size, phase composition (by Spurr-Myers relation) and microstrain. HRTEM was also used with lattice-fringe imaging and selected-area electron diffraction (SAED) to study the particle morphology and crystal structure on the single-particle level. The UV-Vis-NIR diffuse reflectance spectroscopy (DRS; 200-800 nm) was also carried out and the optical band gap was estimated by the Kubelka-Munk/Tauc plot analysis.

### *2.4 Carwash Wastewater Characteristics*

International Journal of Engineering Research & Technology (IJERT)
ISSN: 2278-0181
Vol. 15 Issue 08 , August - 2026

The model pollutant matrix was prepared with car wash effluent. The raw wastewater contained a high dissolved organic load. The baseline (untreated) physicochemical profile is shown in Table 1 and is used as the standard $C_0$ reference for all kinetic and percent-removal calculations. The predicted composition of a filtered or settled carwash effluent is a baseline pH (7.6) that is nearly neutral, with relatively low turbidity (20 NTU) and a residual pollutant load dominated by dissolved and colloidal detergent-derived organics rather than coarse suspended particles. While the effluent is colourless, high UV254 absorbance (2.066 $cm^{-1}$) indicates a high concentration of chromophores having aromatic and conjugated-double-bond structures, providing a clear analytical window to monitor the kinetics of chromophore cleavage during the irradiation period.

**Table 1. Baseline physicochemical characteristics of the raw carwash wastewater.**

| Parameter | Value | Unit |
|---|---|---|
| Total Organic Carbon (TOC) | 51.4 | mg/L |
| Chemical Oxygen Demand (COD) | 620 | mg/L |
| UV254 Absorbance | 2.066 | $cm^{-1}$ (a.u.) |
| Colour | Colourless | — |
| pH | 7.6 | — |
| Turbidity | 20 | NTU |

### *2.5 Reactor Setup and Experimental Procedure*

The photocatalytic degradation tests were performed in a laminar-air-flow (LAF) chamber under 15 W UV-C light to avoid external contamination. Each trial involved dosing 100 mL of carwash effluent with 10, 30, or 50 mg/100 mL of catalyst. Samples were taken at 0, 60, 120 and 180 minutes. Data was generated from three independent experiments (n=3). Control experiments were performed to quantify the net photocatalytic contribution from non-catalytic removal pathways. Two types of control experiments were performed for both catalysts at all three dosages: (i) dark-adsorption experiments where the catalyst was equilibrated with the wastewater for 30 minutes without UV light, and (ii) direct-photolysis experiments with UV-C irradiation and no catalyst, sampled at the same time points.

### *2.6 Analytical Methods and Kinetic Analysis*

TOC, COD, and UV254 absorbance were measured for each sample. Percentage removal (R, %) at any time t was calculated as $R = [(C0 - Ct) / C0] \times 100$, where C0 is the initial concentration/absorbance and Ct is the concentration/absorbance at time t. Mean and standard deviation (SD) were calculated from triplicate measurements for every condition. Pseudo-first-order kinetics, $\ln(C0/Ct) = kapp \times t$, were fitted to the UV254 time-course data (0-180 min) for each catalyst-dose combination; the slope of the linear regression gave the apparent rate constant kapp ($min^{-1}$), from which the half-life was calculated as $t_{1/2} = \ln(2)/kapp$.

## 3. RESULTS AND DISCUSSION

### *3.1 Structural Characteristics: XRD Phase Composition and Crystallite Size*

Both catalysts diffract as a two-phase anatase (JCPDS 21-1272) / rutile (JCPDS 21-1276) mixture, with no brookite or other secondary phase detected (Figs. 1, 2). Undoped $TiO_2$ shows anatase (101), (004), (200), (105), and (211) at $2\theta = 25.22°$, 37.68°, 47.96°, 53.79°, and 54.99° and rutile (110), (101), (111), (211), and (220) at 27.36°, 35.98°, 41.15°, 54.23°, and 56.54°, with rutile (110) as the single most intense peak—rutile is clearly the dominant phase at this 700°C calcination temperature. In 0.5% Ag-$TiO_2$, the same reflections appear at closely similar angles (anatase 25.26–55.02°; rutile 27.39–56.57°), but their relative intensities are inverted: anatase (101) is now the most intense peak, with rutile (110) markedly suppressed.

International Journal of Engineering Research & Technology (IJERT)
ISSN: 2278-0181
Vol. 15 Issue 08 , August - 2026

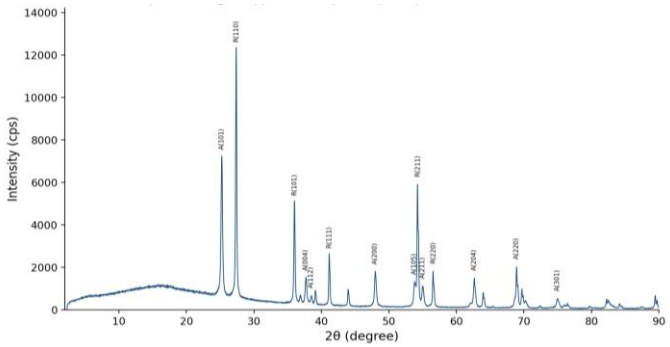


**Fig. 1. XRD pattern of undoped $TiO_2$ (A = anatase, R = rutile).**

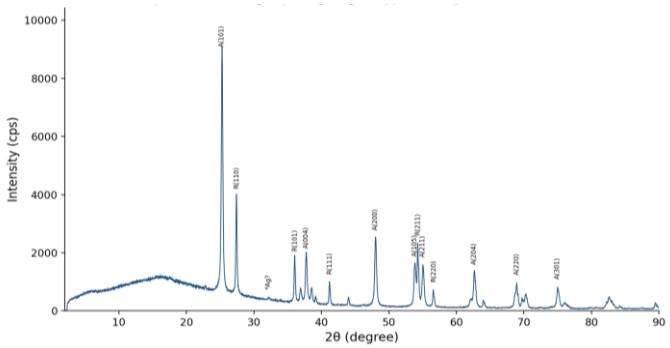


**Fig. 2. XRD pattern of 0.5% Ag-doped $TiO_2$.**

Phase weight fractions (Spurr-Myers, WR = 1/ (1 + 0.8×IA/IR)) and crystallite sizes (Debye-Scherrer and Williamson-Hall) are summarised in Table 2. Silver incorporation drives a substantial anatase-rutile inversion — from a rutile-dominant undoped material (29.6 wt% anatase) to an anatase-dominant 0.5% Ag-$TiO_2$ (64.8 wt% anatase) — which is the single most significant structural difference between the two catalysts and is consistent with $Ag^+$ inhibiting rutile nucleation/growth during calcination. Crystallite size falls only modestly with doping (W-H anatase: 34.06 → 33.99 nm; rutile: 48.32 → 46.67 nm); both W-H fits give negligible, consistently negative microstrain, indicating that peak broadening is size- rather than strain-dominated (Figs. 3, 4). Refined lattice parameters for both phases in both samples agree with JCPDS references, so 0.5% Ag doping produces no resolvable distortion of the host lattice — consistent with silver residing mainly as a surface/interstitial or highly dispersed species rather than as a bulk substitutional dopant.

**Table 2. XRD-derived phase composition and crystallite size of undoped $TiO_2$ and 0.5% Ag–$TiO_2$.**

| Sample | Anatase (wt%) | Rutile (wt%) | Anatase D (nm) Scherrer / W-H | Rutile D (nm) Scherrer / W-H |
|---|---|---|---|---|
| Undoped $TiO_2$ | 29.6 | 70.4 | 35.5 / 34.06 | 59.7 / 48.32 |
| 0.5% Ag-$TiO_2$ | 64.8 | 35.2 | 34.4 / 33.99 | 56.0 / 46.67 |

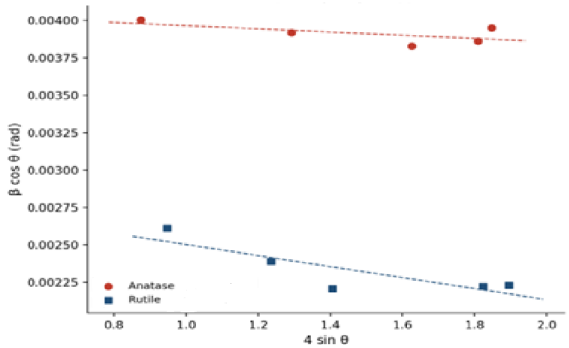


**Fig. 3. Williamson-Hall plots for the anatase and rutile phases Undoped $TiO_2$**

International Journal of Engineering Research & Technology (IJERT)
ISSN: 2278-0181
Vol. 15 Issue 08 , August - 2026

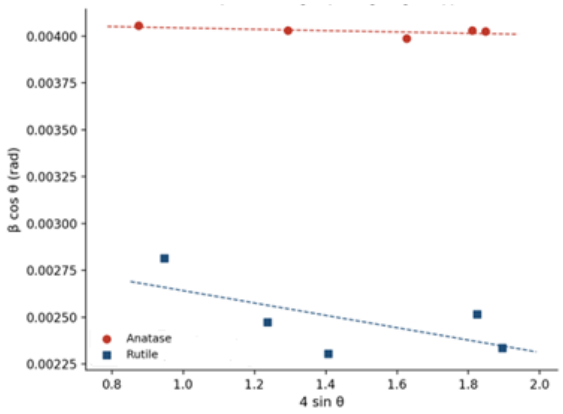


**Fig. 4. Williamson-Hall plots for the anatase and rutile phases of 0.5% Ag-$TiO_2$**

### *3.2 Particle Morphology and Lattice Structure (HRTEM)*

HRTEM (Figs. 5, 6), including lattice-fringe imaging and SAED (Figs. 5, 6), was used to examine both catalysts at the individual-particle level. Undoped $TiO_2$ consists of irregular, polygonal to quasi-spherical primary particles, partially fused into loose agglomerates, with clear, well-resolved lattice fringes confirming high crystallinity. FFT analysis of the fringes gave d-spacings of 3.58 and 3.61 Å, alongside a strong, reproducible 3.36–3.38 Å spacing intermediate between the anatase (101) and rutile (110) references; taken together with the XRD phase composition, the fringes are attributed predominantly to rutile, with minor anatase domains, and the coexistence of both phases within aggregated particles points to heterophase interfaces. SAED shows discrete spots arranged in concentric rings matching $TiO_2$ reference planes, confirming a nanocrystalline, phase-pure material with no detectable secondary phases.

0.5% Ag-$TiO_2$ shows a more open morphology—irregular polygonal-to-quasi-spherical particles together with larger, rounded particles, loosely connected in chain-like/branched arrangements rather than densely fused agglomerates. Lattice fringes are consistent with anatase interplanar spacings, including a clean, strongly resolved 1.695 Å match to anatase (105) (reference 1.699 Å, 0.2% difference); clear grain boundaries and multiple crystallographic orientations confirm a polycrystalline sample. SAED again shows concentric, spot-resolved rings consistent with the strongly anatase-stabilized XRD pattern, with no additional spots or rings attributable to a distinct metallic-Ag or Ag-oxide phase. Overall, the HRTEM dataset corroborates the bulk XRD phase picture at the particle level for both catalysts, and the more loosely connected morphology of 0.5% Ag-$TiO_2$ is consistent with its slightly smaller crystallite size and reduced grain coarsening (Section 3.1).

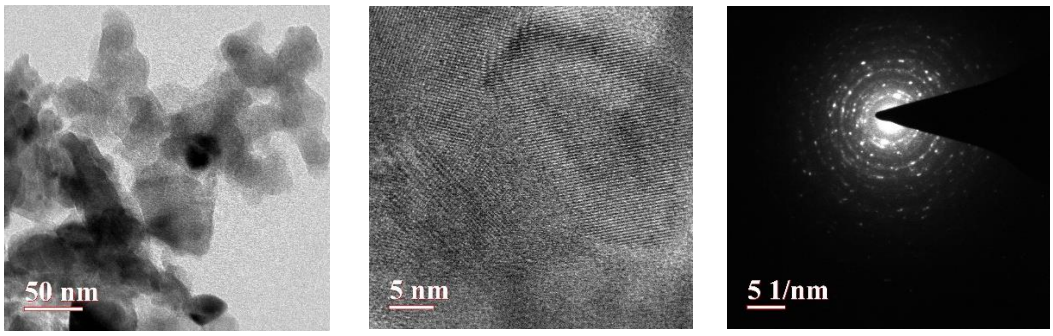


**Fig. 5. HRTEM and SAED images of Undoped $TiO_2$**

International Journal of Engineering Research & Technology (IJERT)
ISSN: 2278-0181
Vol. 15 Issue 08 , August - 2026

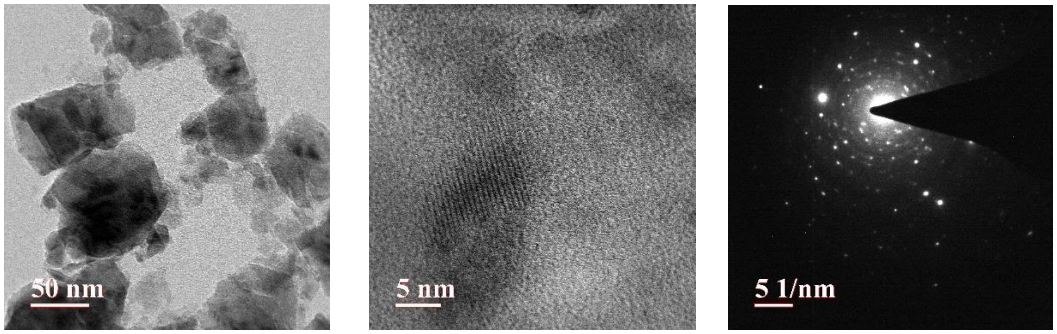


**Fig. 6. HRTEM and SAED images of 0.5% Ag-doped $TiO_2$**

### *3.3 Optical Properties: UV–Vis Diffuse Reflectance Spectroscopy and Band Gap*

Diffuse reflectance spectra (200–800 nm, Figs. 7, 8) show the expected semiconductor profile for undoped $TiO_2$: low, flat UV reflectance (mean 9.6%, 250–340 nm), a sharp absorption edge between 380 and 460 nm (11.8% → 77.9%), and a gradual rise to 94.7% by 800 nm, consistent with negligible visible-light absorption in the absence of dopant states. 0.5% Ag-$TiO_2$ instead shows a markedly higher UV baseline (24.5–26.4%), an edge between 370 and 420 nm, and—distinctively—a flat visible-range plateau (53.5–55.0%, 420–650 nm) followed by a secondary near-infrared upturn beyond 650 nm. No localized dip or peak diagnostic of a classical Ag localized surface plasmon resonance was observed, consistent with the absence of a distinct metallic-Ag phase in the XRD/HRTEM data.

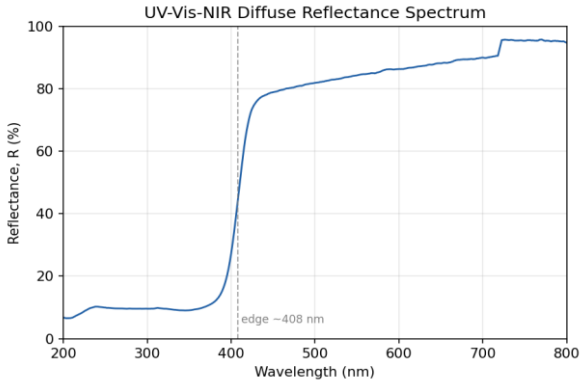


**Fig. 7. UV–Vis–NIR diffuse reflectance spectrum of undoped $TiO_2$ (200–800 nm).**

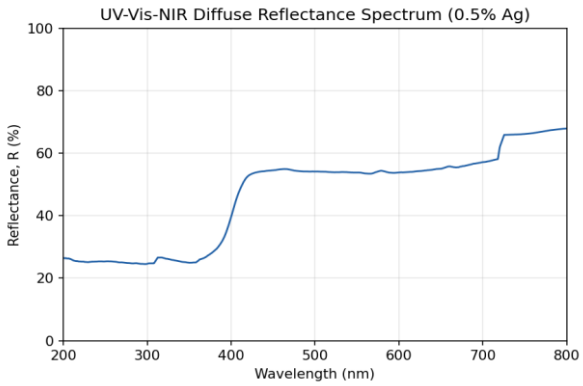


**Fig. 8. UV–Vis–NIR diffuse reflectance spectrum of 0.5% Ag-doped $TiO_2$ (200–800 nm).**

Optical band gaps, extracted from Kubelka-Munk/Tauc plots (indirect transition; Figs. 9, 10) by linear extrapolation of the steepest-slope tangent, are summarised in Table 3. Both samples give an excellent linear Tauc region at 3.07–3.14 eV ($R^2 \geq 0.9999$), and both Tauc-derived values agree closely with an independent, model-free reflectance-midpoint estimate. Undoped $TiO_2$'s band gap (2.96 eV) is somewhat below the ~3.2 eV typical of pure anatase, consistent with its rutile-dominant, mixed-phase character; 0.5% Ag-$TiO_2$'s narrower, flatter gap (2.82 eV) reflects the same mixed-phase averaging together with a persistent, non-plasmonic visible-light absorption background (Kubelka-Munk F(R) ≈ 0.19–0.21 through the visible range, versus near-zero for undoped $TiO_2$),

International Journal of Engineering Research & Technology (IJERT)
ISSN: 2278-0181
Vol. 15 Issue 08 , August - 2026

attributed to the higher anatase fraction and dilute, dispersed silver species rather than to genuine aliovalent lattice doping or an $Ag^0$ plasmonic effect.

**Table 3. Optical band gap of undoped $TiO_2$ and 0.5% Ag–$TiO_2$ (Tauc analysis of UV–Vis DRS).**

| Sample | Tauc Eg (eV) | Tauc $R^2$ | Reflectance-midpoint check |
|---|---|---|---|
| Undoped $TiO_2$ | 2.96 | 0.9999 | 408 nm (3.04 eV) |
| 0.5% Ag-$TiO_2$ | 2.82 | 0.99992 | 400 nm (3.10 eV) |

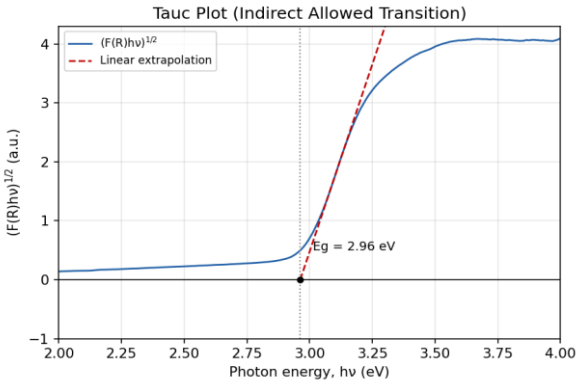


**Fig. 9. Tauc plot (indirect allowed transition) for undoped $TiO_2$.**

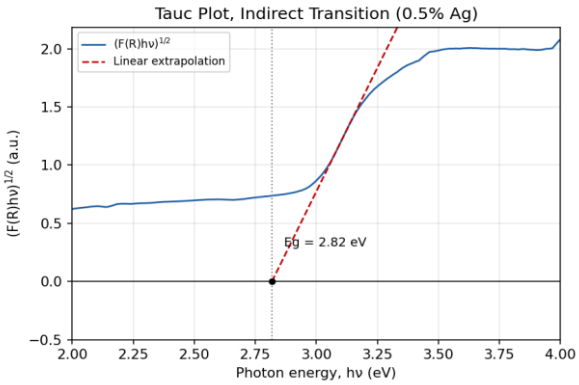


**Fig.10. Tauc plot (indirect allowed transition) for 0.5% Ag-doped $TiO_2$.**

### 3.4 Photocatalytic Performance Evaluation

Across every wastewater-quality indicator monitored, 0.5% Ag–$TiO_2$ left the undoped catalyst well behind, cutting residual COD to 74.6 mg/L against 318.6 mg/L for undoped $TiO_2$ at the best-performing dose. The subsections below quantify the non-catalytic background, the dose/time dependence of removal, and the degradation kinetics, and relate the observed performance gap to the phase-composition and optical differences established in Sections 3.1–3.3.

#### 3.4.1 Non-Catalytic Background: Adsorption and Photolysis

Dark-adsorption (30 min, no UV; Table 4) and direct-photolysis (UV-C only, no catalyst; Table 5) controls were used to isolate genuine photocatalytic removal. Adsorption alone removed only 1.5–3.8% of TOC, 1.6–4.5% of COD, and 3.7–6.5% of UV254 for undoped $TiO_2$, and a still modest 4.5–10.1%, 6.4–12.2%, and 6.9–14.1%, respectively, for 0.5% Ag-$TiO_2$—the higher uptake on the Ag-doped material tracking its greater anatase-derived surface hydroxylation and increasing with dose in both cases. Photolysis alone removed 10.8% TOC, 15.2% COD, and 19.6% UV254 after 180 min. Together, these non-catalytic pathways account for well under a quarter of the removal achieved under illumination (Section 3.4.2), confirming that the degradation reported below is predominantly photocatalytic in origin.

International Journal of Engineering Research & Technology (IJERT)
ISSN: 2278-0181
Vol. 15 Issue 08 , August - 2026

**Table 4. Surface-adsorption (dark) removal after 30 min contact, no UV**

| Catalyst | Dose (mg/100 mL) | TOC Ads. (%) | COD Ads. (%) | UV254 Ads. (%) |
|---|---|---|---|---|
| Undoped $TiO_2$ | 10 | 1.7 | 2.1 | 3.7 |
| Undoped $TiO_2$ | 30 | 3.8 | 4.5 | 4.9 |
| Undoped $TiO_2$ | 50 | 1.5 | 1.6 | 6.5 |
| 0.5% Ag-$TiO_2$ | 10 | 4.5 | 6.4 | 6.9 |
| 0.5% Ag-$TiO_2$ | 30 | 7.7 | 8.9 | 10.6 |
| 0.5% Ag-$TiO_2$ | 50 | 10.1 | 12.2 | 14.1 |

**Table 5. Direct UV-C photolysis control (no catalyst)**

| Time (min) | TOC Removal (%) | COD Removal (%) | UV254 Removal (%) |
|---|---|---|---|
| 0 | 0.0 | 0.0 | 0.0 |
| 60 | 5.7 | 6.0 | 9.3 |
| 120 | 7.6 | 11.7 | 14.8 |
| 180 | 10.8 | 15.2 | 19.6 |

### 3.4.2 Dose and Time Dependence of Degradation

Fig. 11 summarises TOC, COD and UV254 removal at 180 min across the three catalyst doses. 0.5% Ag-$TiO_2$ improved monotonically with dose (COD 71.6 → 79.7 → 88.0% for 10 → 30 → 50 mg/100 mL), as expected from the greater active surface area and photon capture available at higher loading. Undoped $TiO_2$, by contrast, peaked at 30 mg/100 mL (COD 60.0%) and then declined at 50 mg/100 mL (COD 48.6%, below even the 10 mg/100 mL value)—an anomaly consistent with its rutile-dominant, coarser-crystallite structure (Section 3.1), in which particle agglomeration and UV light-screening at higher loading outweigh the benefit of additional catalyst mass. No such ceiling was observed for the anatase-rich 0.5% Ag-$TiO_2$.

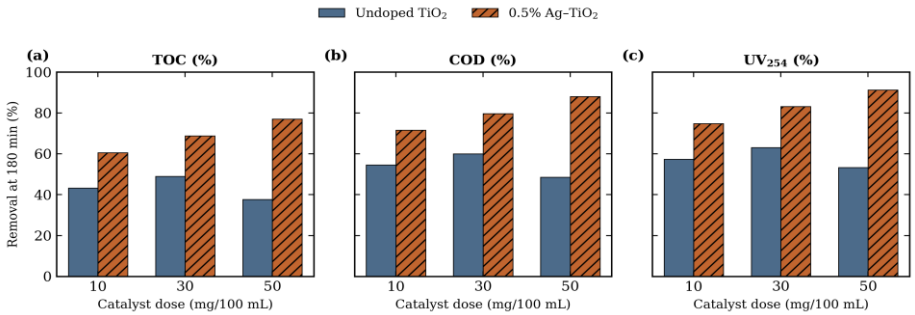


**Fig. 11. Removal of (a) TOC, (b) COD and (c) $UV_{254}$ at 180 min as a function of catalyst dose for undoped $TiO_2$ and 0.5% Ag–$TiO_2$.**

At the practical optimum (50 mg/100 mL, 180 min), residual concentrations were 11.80 ± 0.245 mg/L TOC, 74.6 ± 2.91 mg/L COD, and 0.182 ± 0.0060 $cm^{-1}$ UV254 for 0.5% Ag-$TiO_2$, versus 32.03 ± 0.197 mg/L, 318.6 ± 3.20 mg/L, and 0.965 ± 0.0490 $cm^{-1}$ for undoped $TiO_2$—roughly a two-fold improvement on every measure. For both catalysts, removal consistently followed UV254 > COD > TOC at every dose (e.g., 91.2 > 88.0 > 77.0% for 0.5% Ag-$TiO_2$ at 50 mg/100 mL), reflecting the expected oxidation sequence: rapid cleavage of UV254-active aromatic/conjugated chromophores, followed by progressive oxidation of the resulting fragments (COD), with complete mineralization to $CO_2$ and $H_2O$ (TOC) lagging as some partially oxidized intermediates persist beyond 180 min.

International Journal of Engineering Research & Technology (IJERT)
ISSN: 2278-0181
Vol. 15 Issue 08 , August - 2026

### 3.4.3 Kinetic Behaviour

Pseudo-first-order fits to the UV254 decay (ln(C0/Ct) vs. t) were good at every catalyst-dose combination ($R^2$ = 0.90–0.99, Table 6, Fig. 12), consistent with Langmuir-Hinshelwood behaviour at the low pollutant concentrations present. Rate constants track the endpoint removal closely: 0.5% Ag-$TiO_2$ increased monotonically with dose (7.55 → 9.67 → 13.10 × $10^{-3}$ $min^{-1}$), reaching a half-life of 52.9 min at 50 mg/100 mL — roughly three times faster than undoped $TiO_2$ at the same dose (4.25 × $10^{-3}$ $min^{-1}$, $t_{1/2}$ ≈ 163 min) — while undoped $TiO_2$'s rate constant, mirroring its endpoint removal, peaks at 30 mg/100 mL (5.50 × $10^{-3}$ $min^{-1}$) before falling at 50 mg/100 mL, the kinetic signature of the same dosage-inhibition effect. The consistently higher rate constants and higher ultimate removal for 0.5% Ag-$TiO_2$ track directly with its substantially higher anatase content (Section 4.1) and reduced visible/UV recombination losses (Section 3.3), tying the photocatalytic performance gap back to the underlying phase composition and optical differences between the two catalysts.

**Table 6. Pseudo-first-order rate constants (UV254 basis), coefficients of determination and half-lives.**

| Catalyst | Dose (mg/100 mL) | kapp (×$10^{-3}$ $min^{-1}$) | $R^2$ | $t_{1/2}$ (min) |
|---|---|---|---|---|
| Undoped $TiO_2$ | 10 | 4.711 | 0.9851 | 147.1 |
| Undoped $TiO_2$ | 30 | 5.501 | 0.9794 | 126.0 |
| Undoped $TiO_2$ | 50 | 4.245 | 0.9763 | 163.3 |
| 0.5% Ag-$TiO_2$ | 10 | 7.551 | 0.9612 | 91.8 |
| 0.5% Ag-$TiO_2$ | 30 | 9.670 | 0.9395 | 71.7 |
| 0.5% Ag-$TiO_2$ | 50 | 13.102 | 0.8999 | 52.9 |

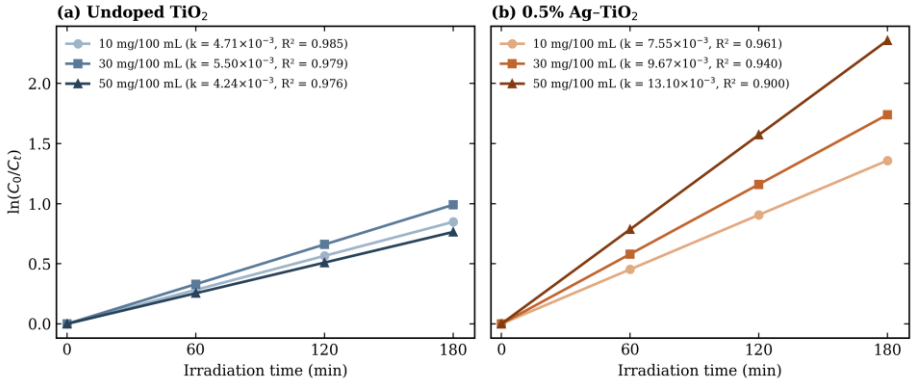


**Fig. 12. Pseudo-first-order kinetic plots [ln($C_0/C_t$) vs. t] for $UV_{254}$ degradation at all three catalyst doses: (a) undoped $TiO_2$, (b) 0.5% Ag–$TiO_2$.**

## 4. CONCLUSION

Undoped and 0.5% Ag-doped $TiO_2$ catalysts were synthesized by the microwave-assisted sol-gel method using agar-agar as a green templating agent for direct comparison of photocatalytic activity in carwash wastewater treatment. XRD analysis revealed a significant phase inversion from rutile to anatase after silver incorporation from a rutile-dominant undoped material (29.6 wt% anatase / 70.4 wt% rutile) to an anatase-dominant 0.5% Ag-$TiO_2$ (64.8 wt% anatase / 35.2 wt% rutile). This was accompanied by a modest reduction in crystallite size (Williamson-Hall: anatase 34.06 → 33.99 nm; rutile 48.32 → 46.67 nm) and a narrowed optical band gap (2.96 → 2.82 eV, as determined by Tauc analysis of UV-Vis diffuse reflectance spectra). HRTEM lattice-fringe analysis further supported the anatase-dominant character of the Ag-doped $TiO_2$ catalysts at the particle level, with no evidence from either XRD or HRTEM/SAED of a distinct, well-crystallized metallic silver phase. These structural and optical modifications resulted in a significantly higher removal efficiency for 0.5% Ag-$TiO_2$ compared to undoped $TiO_2$ across all three water-quality parameters monitored at the optimal dose of 50 mg/100 mL (TOC 77.0% vs. 37.7%; COD 88.0% vs. 48.6%; UV254 91.2% vs. 53.3%), alongside an approximately 3.1-fold increase in the pseudo-first-order UV254 rate constant (13.10 vs. 4.25 × $10^{-3}$ $min^{-1}$). Control experiments confirmed that this enhancement is indicative of genuine semiconductor-mediated photocatalysis, rather than non-catalytic photolysis or surface adsorption, both of which contributed only marginally to overall removal. Moreover, the degradation

International Journal of Engineering Research & Technology (IJERT)
ISSN: 2278-0181
Vol. 15 Issue 08 , August - 2026

efficiency of the undoped $TiO_2$ decreased abnormally at the highest used dose (50 mg/100 mL). These results demonstrate that 0.5% Ag-$TiO_2$ is a much better and cheaper photocatalyst than unmodified $TiO_2$ for advanced oxidation treatment of carwash wastewater and justify the further testing of this material at pilot scale as a part of an integrated wastewater reuse treatment train.

## ACKNOWLEDGMENT

The authors thank the Department of Chemistry, Agra College, Dr. Bhim Rao Ambedkar University, Agra, for synthesis facilities and MNIT Jaipur, Jiwaji University Gwalior, SAIF IIT Bombay, Central University of Jammu, and Foodtech Lab, Agra for characterisation support.

## REFERENCES

[1] Bhatti, Z. A., Mahmood, Q., Raja, I. A., Malik, A. H., Khan, M. S., & Wu, D. (2011). Chemical oxidation of carwash industry wastewater as an effort to decrease water pollution. *Physics and Chemistry of the Earth, Parts A/B/C*, *36*, 465–469.

[2] Chakhtouna, H., Benzeid, H., Zari, N., Qaiss, A. E. K., & Bouhfid, R. (2021). Recent progress on Ag/$TiO_2$ photocatalysts: Photocatalytic and bactericidal behaviors. *Environmental Science and Pollution Research*, *28*, 44638–44666.

[3] Fall, C., López-Vázquez, C. M., Jiménez-Moleon, M. D. C., Bâ, K. M., Díaz-Delgado, C., García-Pulido, D., & Lucero-Chavez, M. (2007). Carwash wastewaters: characteristics, volumes, and treatability by gravity oil separation. *Revista Mexicana de Ingeniería Química*, *6*(2), 175-184.

[4] Ganiyu, S. O., Vieira dos Santos, E., Tossi de Araújo Costa, E. C., & Martínez-Huitle, C. A. (2018). Electrochemical advanced oxidation processes (EAOPs) as alternative treatment techniques for carwash wastewater reclamation. *Chemosphere*, *211*, 998–1006.

[5] Hernández, R., Hernández-Reséndiz, J. R., Cruz-Ramírez, M., Velázquez-Castillo, R., Escobar-Alarcón, L., Ortiz-Frade, L., & Esquivel, K. (2020). Au-$TiO_2$ synthesized by a microwave-and sonochemistry-assisted sol-gel method: Characterization and application as photocatalyst. *Catalysts*, *10*(9), 1052.

[6] Huang, J., Guo, X., Wang, B., Li, L., Zhao, M., Dong, L., Liu, X., & Huang, Y. (2015). Synthesis and photocatalytic activity of Mo-doped $TiO_2$ nanoparticles. *Journal of Spectroscopy*, *2015*, Article 681850.

[7] Imoisili, P. E., Jen, T. C., & Safaei, B. (2021). Microwave-assisted sol–gel synthesis of $TiO_2$-mixed metal oxide nanocatalyst for degradation of organic pollutant. *Nanotechnology Reviews*, *10*, 126–136.

[8] Lu, C.-H., Li, K.-C., Balaji, S., & Senthil Kumar, P. (2021). Agar-assisted sol-gel synthesis and electrochemical characterization of $TiNb_2O_7$ anode materials for lithium-ion batteries. *Ceramics International*, *47*(Part A).

[9] Rabhi, S., Belkacemi, H., Bououdina, M., Kerrami, A., Ait Brahem, L., & Sakher, E. (2019). Effect of Ag doping of $TiO_2$ nanoparticles on anatase-rutile phase transformation and excellent photodegradation of amlodipine besylate. *Materials Letters*, *236*, 640–643.

[10] Sarmadi, M., Foroughi, M., Najafi Saleh, H., Sanaei, D., Zarei, A. A., Ghahrchi, M., & Bazrafshan, E. (2020). Efficient technologies for carwash wastewater treatment: A systematic review. *Environmental Science and Pollution Research*, *27*, 34823–34839.

[11] Singh, A., & Kumar, S. (2021). Effect of Ag doping on phase-change and photocatalytic performance of rutile–anatase mixed-phase titanium dioxide ($TiO_2$) nanoparticles. *Applied Physics A*, *127*, Article 839.

[12] Suwarnkar, M. B., Dhabbe, R. S., Kadam, A. N., & Garadkar, K. M. (2014). Enhanced photocatalytic activity of Ag-doped $TiO_2$ nanoparticles synthesized by a microwave-assisted method. *Ceramics International*, *40*(4), 5489–5496.

[13] Thamaphat, K., Limsuwan, P., & Ngotawornchai, B. (2008). Phase characterization of $TiO_2$ powder by XRD and TEM. *Kasetsart Journal (Natural Science)*, *42*(5), 357–361.

[14] Zhang, J., Zhou, P., Liu, J., & Yu, J. (2014). New understanding of the difference of photocatalytic activity among anatase, rutile, and brookite $TiO_2$. *Physical Chemistry Chemical Physics*, *16*(38), 20382–20386.